PROTEINS
STRUCTURE ■ FUNCTION ■ BIOINFORMATICS

Calcium binding to the purple membrane: A molecular dynamics study

Tsjerk A. Wassenaar,[1] Xavier Daura,[2] Esteve Padrós,[3] and Alan E. Mark[1,4]*

[1] Department of Biophysical Chemistry, Groningen Biomolecular Sciences and Biotechnology Institute (GBB), University of Groningen, 9747 AG Groningen, The Netherlands

[2] Catalan Institution for Research and Advanced Studies (ICREA) and Institute of Biotechnology and Biomedicine (IBB), Universitat Autònoma de Barcelona, E-08193 Bellaterra, Spain

[3] Unitat de Biofísica, Departament de Bioquímica i de Biologia Molecular, Facultat de Medicina and Centre d'Estudis en Biofísica, Universitat Autònoma de Barcelona, E-08193 Bellaterra, Spain

[4] School of Molecular and Microbial Sciences and the Institute of Molecular Biosciences, University of Queensland, Brisbane, Queensland 4072, Australia

ABSTRACT

The purple membrane (PM) is a specialized membrane patch found in halophilic archaea, containing the photoreceptor bacteriorhodopsin (bR). It is long known that calcium ions bind to the PM, but their position and role remain elusive to date. Molecular dynamics simulations in conjunction with a highly detailed model of the PM have been used to investigate the stability of calcium ions placed at three proposed cation binding sites within bR, one near the Schiff base, one in the region of the proton release group, and one near Glu9. The simulations suggest that, of the sites investigated, the binding of calcium ions was most likely at the proton release group. Binding in the region of the Schiff base, while possible, was associated with significant changes in local geometry. Calcium ions placed near Glu9 in the interior of bR (simultaneously to a Ca^{2+} near the Schiff base and another one near the Glu194–Glu204 site) were not stable. The results obtained are discussed in relation to recent experimental observations and theoretical considerations.

Proteins 2009; 74:669–681.

Key words: bacteriorhodopsin; cation binding; bond valence sum; simulation; model.

INTRODUCTION

Bacteriorhodopsin (bR) is a light harvesting protein found in certain species of halophilic archaea. bR absorbs green light (500–650 nm, maximum absorbance 568 nm), giving rise to an intense purple color that can cause the salt lakes and pools where the archaea are found to appear purple. bR is localized within specific patches on the cell surface, called the purple membrane (PM). The PM is a two-dimensional crystal with an almost perfect hexagonal lattice and a high protein to lipid ratio. bR is the sole protein found in the PM, which also has a lipid composition that is distinct from the rest of the archaeal membrane. The PM and bR have been the focus of intense study since first isolated in 1970.[1] This is primarily because, as a member of the seven transmembrane helical (7TM) protein superfamily, bR is closely related to G-protein coupled receptors, many of which are important targets for pharmaceutical intervention. This together with the ease with which large quantities of protein can be obtained, means that bR is widely used as a model for the understanding of sensing and signaling by 7TM receptors.

Functional bR consists of a protein, bacterioopsin, and a chromophore, retinal, which are covalently linked via the formation of a Schiff base between retinal and Lys216. On absorption of green light the chromophore isomerizes from an *all-trans* form to a *13,14-cis* configuration. This initiates a series of deprotonation–protonation events, resulting in the effective translocation of a proton from the intracellular matrix to the exterior of the cell. In this way, the action of light on bR results in the establishment of a proton gradient across the membrane, which is in turn used to drive ATP-synthesis. A longstanding question regarding bR and the PM is the location and role of divalent cations. It is well established that under physiological conditions, a number of calcium and magnesium ions are bound to the PM,[2–4] and that the presence of these cations is required to maintain the activity of the PM at low pH. Acidification of the PM[2,5] results in a shift

Additional Supporting Information may be found in the online version of this article.

Tsjerk A. Wassenaar's current address is Biomolecular NMR Spectroscopy, Bijvoet Center, Utrecht University, Padualaan 8, 3584 CH Utrecht, The Netherlands.

Grant sponsor: Dirección General de Investigación (MCYT); Grant numbers: BMC2003-04941, BFU2006-04656BMC; Grant sponsor: TOP Grant 700.53.309 Netherlands Organisation for Scientific Research (NWO).

*Correspondence to: Alan E. Mark, School of Molecular and Microbial Sciences and the Institute of Molecular Biosciences, University of Queensland, Brisbane, QLD 4072, Australia. E-mail: a.e.mark@uq.edu.au

Received 11 January 2008; Revised 8 May 2008; Accepted 19 May 2008
Published online 14 August 2008 in Wiley InterScience (www.interscience.wiley.com). DOI: 10.1002/prot.22182

in the absorption spectrum λ_{max} of bR from 570 nm (purple) to 620 nm (blue) and coincides with a loss of proton pumping functionality. This has been ascribed to the protonation of Asp85,[6–8] the key residue in the first of a series of proton transfer steps. The removal of membrane associated cations by chelation[2] or by deionization[2] results in a shift in this response by about 3 pH units[2] because of the increase of the pK_a of Asp85.

Several studies have suggested that the effect of cations is the result of nonspecific binding to the lipids of the PM, for example, by competing with associated protons and raising the pK_a of the lipid head groups, otherwise known as the Gouy-Chapman effect.[9–12] The resulting change in the concentration of protons at the membrane surface would then account for the deprotonation of Asp85. Support for nonspecific binding comes from work such as that of Váró *et al.*[12] suggesting that cations bind with equal affinity to both the extracellular and intracellular membranes. However, it has been argued that the findings of Váró *et al.*[12] may result from the rapid equilibration of proton concentrations on both sides of the membrane,[13] preventing the measurement of differences in the cytoplasmic and extracellular surface pH.[14] In addition, it has been shown that the predictions from the Gouy-Chapman model do not correspond with experimental observations.[15]

Other data suggest that divalent cations bind to specific locations in or around bR. For example, several groups have proposed that a location near Asp85 in the retinal pocket of bR is the critical cation binding site.[4,16,17] The possibility of a binding site in this region is supported by a number of studies, including recent EXAFS/XANES results[18–21] and would be consistent with results obtained from one- and two-photon spectroscopy.[16,22] There is also much evidence against binding at such a location.[23,24] For example, Fu *et al.*[23] showed that the purple color could be reconstituted even with large cations, which would not be expected to occupy a position in the region of the Schiff base. However, the most compelling evidence against the binding of cations in the interior of bR comes from the fact that in none of the high-resolution crystal structures it has been possible to definitely identify a cation bound in the vicinity of the chromophore. Some density is observed in the structure solved by Mitsuoka *et al.* 2AT9,[25] which the authors argued was associated with a positive charge. Although this structure was solved at a relatively low resolution, (3.0 Å) it does leave open the question of whether the crystallization procedure and/or conditions used to obtain the high resolution structures could have resulted in the loss of the associated cations.

In addition to the retinal binding pocket, a number of other potential binding sites on the extracellular side of bR have been proposed. Among the sites suggested are a position directly associated with the proton release group, formed by Glu194 and Glu204, and a site in the vicinity of Glu9, which is connected to the proton release group by a network of water molecules.[21,26] Still, others have proposed that the most likely specific binding sites are on the protein–lipid interface, rather than in the interior of the protein. Results obtained using electron paramagnetic resonance (EPR) suggest that a high-affinity binding site was located at a distance of 9.8 $\pm$ 0.7 Å of Glu74.[14] This finding is consistent with results obtained from ^{13}C NMR,[27] which pointed to a location at the protein–lipid interface in the region between helices F and G, close to Ala196.

Here, we present the results of molecular dynamics simulations designed to investigate whether calcium ions could bind at any of the proposed interior positions. Over the past decade, many molecular dynamics simulations and quantum mechanical studies of bR have been performed. These have focused primarily on the role of internal water molecules,[28–30] retinal isomerization,[31] and the initial stages in proton translocation.[32–35] The models used for these studies have included isolated bR molecules,[21,36] single bR molecules in an argon slab[37] or in a DMPC bilayer,[38] bR trimers immersed in a bilayer of POPC lipids,[28,29] and a single bR molecule in a disc of DPPC lipids, surrounded by truncated lipoproteins.[39] For the current work, the use of a complete model including the characteristic lipids was essential. The system constructed for this study resembles the near complete model of the PM used by Baudry *et al.*[30] The primary difference is that in the current work, the nature and position of the lipids has been based where possible on experimental data[40–42] and that the system simulated consisted of three bR trimers to minimize possible artifacts because of periodicity.

The binding of calcium ions at three putative binding sites has been investigated. The sites include the Schiff base region, as proposed by Jonas and Ebrey,[6] Stuart *et al.*,[16] Pardo *et al.*,[17] and Sepulcre *et al.*,[18,21] the proton release group, as suggested by Sepulcre *et al.*[21] and Sanz *et al.*,[26] and a site in the interior of bR near Glu9 as proposed by the same group. These sites are the locations in the interior of bR. The primary aim was to investigate if a calcium ion could be accommodated at the sites proposed without major disruption of the local geometry. The results are discussed in terms of the stability and the relationship between the configurations obtained in the simulations and the available crystal structures. Finally, the findings are discussed in relation to a range of experimental observations and theoretical considerations.

METHODS

The simulation model

Construction of the model

The construction of the model largely followed the approach taken by Baudry *et al.*[30] The primary improvements over this earlier model relate to the type and place-

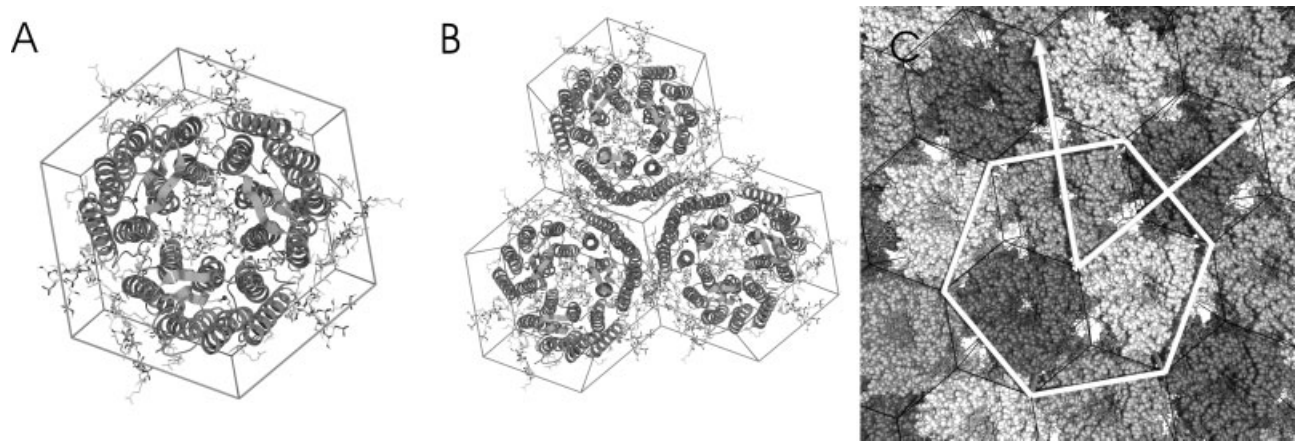

Figure 1

A pictorial representation of the model of the purple membrane simulated. (**A**) The hexagonal unit cell, showing the arrangement of bacteriorhodopsin (bR), S-TGA-1, PGP-Me, and Squalene. (**B**) The simulation system containing three bR trimers with associated lipids. (**C**). A view of the simulation system, showing the three bacteriorhodopsin trimers with associated lipids, surrounded by periodic images. Note, each trimer is in direct contact interacts with the other two trimers but not with its own periodic image. The lattice vectors of the simulation system as well as the regular hexagonal prism derived from these lattice vectors are indicated. All figures were created with PyMOL[43] and POV-Ray.[44]

ment of the lipids. The basic hexagonal unit cell is shown in Figure 1(A). This unit, which contains a bR trimer and its associated lipids, was constructed using information from three different crystal structures, namely, 1BRR—a bR trimer, resolved to 2.9 Å resolution[45]; 1QHJ—a bR monomer, resolved to 1.9 Å resolution[46]; and 1C3W—a bR monomer, resolved to 1.55 Å resolution.[47]

The structure of the bR trimer (1BRR) formed the basis of the model. The three bR units of this structure have a number of structural differences. In particular, coordinates are not available for a number of atoms and residues. The missing side chain atoms of a number of residues (residues 3, 225, 227, 229, 230, and 232 of chain A, residues 3, 4, 227, and 232 of chain B, and residues 1, 227, 229, 230, and 232 of chain C) were modeled using the SwissPDB Viewer.[48] The first two residues of the N-termini of chains A and B are not resolved in the crystal structure were modeled, based on the configuration of these residues in chain C. The N-terminal glutamine group was modeled as pyroglutamic acid. As the C-termini were not resolved for any of the chains, residues after Glu232 were omitted from the system.

The protonation states of titratable residues were chosen according to their normal protonation states at pH 7.0 except for Asp96 and Asp115, which were protonated as appropriate for bR in the ground state. In two of the simulations the proton release group was also protonated, in order to mimic the effect of a protonated water cluster.[49]

Lipid composition

Despite several studies by different groups, the exact lipid composition of the PM is still uncertain.[40–42] The main constituents are known to be PGP (-Me), S-TGA-1 (sulphated triglycosyl diphytanylglycerol), and squalene, but the precise ratio of each of these compounds to bR is debated. Neutron diffraction experiments support that there being two glycolipid S-TGA-1 molecules per unit bR one in the intratrimer space and one in the intertrimer space.[50] S-TGA-1, a glycolipid, contains three sugar moieties linked to an archeol group. These sugar groups are in order from the archeol: 1,2-α-D-glucose, 1,6-α-D-mannose, and 1-β-D-galactose-3-sulfate. The head groups of the intratrimer glycolipids are resolved in the structure 1BRR. The glycolipid in the intertrimer space corresponds to the diphytanoyl chain numbered 501 in the structure 1QHJ. The head group of the intratrimer S-TGA-1 unit was modeled onto this lipid tail, avoiding van der Waals contacts with either neighboring lipids or the protein.

The S-TGA-1 molecules account for two of the lipids that are resolved in the crystal structures. The other phytanoyl lipids that are resolved in the crystal structures were assigned to be PGP-Me. A total of seven PGP-Me molecules per unit bR were added to the system, six of which were placed based on the positions of the diphytanoyl-glycerol tails (502–507) resolved in the structure 1QHJ. Three additional PGP-Me moieties (one for each BR unit) were added in the intratrimer region on the intracellular side. The PGP-Me head group was modeled using the PRODRG server.[51] The head group of each of the diphytanoyl-glycerol chains was modeled so as to maximize the space between neighboring head groups and to avoid van der Waals contacts with either neighboring lipids or the protein.

The conformation and position of the third lipid constituent, squalene, was taken from structure 1C3W. In 1C3W, the squalene molecule lies in an S-like conformation close to the side of bR. The side chain methyl groups which are not resolved in the structure were modeled based on standard geometries.

Bound waters

A network of water molecules within bR, which is believed to be involved in proton translocation, is resolved in several of the crystal structures. As the positions of the crystal waters in the structure 1C3W[47] coincide with the positions predicted based on free energy perturbation calculations,[30] the crystal waters as observed in this structure were incorporated into the model.

Lattice vectors

The PM is a quasi two-dimensional crystalline system, in which each hexagonal unit cell contains three bR molecules together with their associated lipid molecules. In the simulations, the system was also treated as a two-dimensional lattice. As shown in Figure 1(B,C), the final system consisted of three hexagonal cells containing a total of nine bR molecules. The system was also periodic in the direction perpendicular to the plane membrane. The initial distance between adjacent layers was 7.6 nm, which was sufficient to ensure that the layers did not interact directly, and the solvent between the layers showed bulk-like behavior. Three unit cells were simulated in order to reduce the effect of the periodic boundary conditions within the plane of the membrane and to provide greater statistics. We note that, in addition to being more realistic, it is computationally more efficient to simulate a fully periodic PM, than to simulate either an isolated monomer or trimer of bR in a lipid bilayer.

Solvent

The space between the membrane layers was filled with water. As the electronic properties of bR as well as the stability and dynamics of the PM itself are dependent on the ionic strength of the environment, sufficient sodium and chloride ions were added to give a salt concentration of $\sim$3.3*M*, conditions under which the PM is known to be stable.[52]

Force field parameters

The protein was described using the GROMOS96 43a2 united atom force field.[53,54] Parameters for retinal and the Schiff base Lys216 were taken from Kandt *et al.*[29] Parameters for squalene, the lipid tails, the head group of PGP-Me were taken from equivalent chemical groups within phospholipids described within the GROMOS96 43a2 force field.[53,54] Parameters for the carbohydrate moieties of S-TGA-1 were based on the parameters derived for the GROMOS96 45a3 force field,[55] which are fully compatible with the 43a2 force field (Roberto Lins, personal communication). The building blocks for 1,4-α-D-glucose and 1,4-β-D-glucose from this force field were adapted to form the corresponding 1,2-α-D-glucose, 1,6-α-D-mannose, and 1,3-β-D-galactose. Water molecules were described using the Simple Point Charge (SPC) model.[56]

The complete description of the solvated PM, including the structure file containing nine bR molecules and the associated lipids, as well as the topology files, are available as supplementary material. The structure file contains $\sim$52k atoms in total.

Simulations

General

All simulations were performed using the Gromacs package[57–59] version 3.1.4. Nonbonded interactions were evaluated using a twin range cutoff of 0.9 and 1.4 nm together with a reaction field (RF) correction[60] to correct for the neglect of electrostatic interactions beyond the longer range cutoff ($\varepsilon_{RF} = 78.0$). Interactions within the shorter range cutoff were evaluated at every step, whereas interactions within the longer range cutoff were evaluated every 10 steps. These parameters correspond to the conditions under which the force-field parameters were derived.[53,54] The temperature was maintained at 300 K by applying a Berendsen thermostat.[61] The protein/membrane and solvent were coupled independently to the heat bath with a coupling time of 0.1 ps. The pressure was weakly coupled to a reference pressure of 1 bar using an anisotropic Berendsen barostat,[61] with a coupling time of 1.0 ps and a compressibility of 4.6×10^{-5} bar^{-1}. The time step used for integration of the equations of motion was 0.002 ps. The bond lengths and angle of the water molecules were constrained using the SETTLE algorithm.[62] Bond lengths within the proteins and lipids were constrained using the SHAKE algorithm.[63]

Calcium ions positioned at putative binding sites

The simulations performed are listed in Table I. In system **1**, a single calcium ion was placed in the interior of each bR unit near the Schiff base (P1) between Asp85 and Asp212. In system **2**, a single calcium ion was placed in the region of the proton release group between Glu194 and Glu204. Both Glu194 and Glu204 were deprotonated. In system **3**, three calcium ions per bR unit were added, one near Asp85 (P1), one near the proton release group Glu194/Glu204 (P2), and one next to Glu9 (P3). In this case, Glu 194 in the proton release group was protonated. System **4** was identical to system **3**, except that Glu 194 was deprotonated (as in system **2**). Note that the calcium ions were placed such that the overlap with the surrounding atoms was minimized.

Table I
An Overview of the Simulations Performed

System	Description	Remarks	Length
1	Calcium ion positioned at P1	Glu 194 protonated	20 ns
2	Calcium ion positioned at P2	Glu 194 deprotonated	20 ns
3	Calcium ions positioned at P1, P2, and P3	Glu 194 protonated	20 ns
4	Calcium ions positioned at P1, P2, and P3	Glu 194 deprotonated	20 ns

After the calcium ions were added, each system was first energy minimized, and then simulated for 10 ps with position restraints on all heavy atoms within bR to relax the system. After a further 10 ps of simulation without restraints, the 20 ns production runs were performed.

Analysis

Comparison with crystal structures

The simulation results were compared to the available crystal structures (PDB entries IDs 1AP9,[64,65] 1AT9,[66] 1BRR,[45] 1BRX,[67] 1C3W,[47] 1FBB,[68] 1IW6,[69] 1KGB,[70] 1M0L,[71] 1PY6,[72] 1QHJ,[46] 1QM8,[73] 1XJI,[74] 2AT9,[25] and 2BRD[75]). Note that the structure 1AP9 used in this work has been corrected for 18% twinning in the crystals.[65] The comparison focused on the local geometry in the region of the proposed calcium binding sites P1, P2, and P3, as expressed in a set of distances between key residues. To illustrate the results, a representative structure was extracted from each simulation. This structure was chosen based on the local geometry in the vicinity of the calcium ion so as to best represent the local structure sampled in a given simulation. To determine the representative structure, a distance matrix of selected atoms from the key residues (putatively) involved in calcium binding or the catalytic site (the Schiff base region) was defined for each site (Table II). The elements of these distance matrices were evaluated for each individual bR unit in each frame of the trajectory. An average distance matrix was then determined for each simulation. The structure for which the sum of the square of the deviations of the elements of the corresponding distance matrix to the average matrix was a minimum (i.e., the structure closest to the average overall) was taken as a representative structure. To verify that the results obtained using the representative structures reflected the results of the simulations, overall the analysis was repeated using an ensemble of structures extracted from the trajectories. The results of this analysis are presented as supplementary data.

Bond valence sums

To help quantify the coordination state of the calcium ion and to provide a measure of the interaction of each calcium ion with its surroundings, an apparent bond valence contribution was calculated for each oxygen atom lying within 0.5 nm of the calcium ion. By summing the individual contributions, an overall bond valence sum could then be determined for each calcium ion. The bond valence sum traces back to the work of Pauling[76] and has previously been used to investigate calcium binding in proteins[77] and for analysis of the interactions between Na^+ and a protein in molecular dynamics simulations.[78] The method uses the empirical relationship between the cation–ligand distance and the bond order, under the assumption of locally neutralizing charges. As such, it can be used to assess the quality or 'fitness' of binding of a cation at a certain position in a protein: a

Table II
Average Distances and Standard Deviations Between Calcium Ions and Selected Atom

		Calcium ion (system:position)											
Residue:	Atom	1:P1		2:P2		3:P1		3:P2		4:P1		4:P2	
E9:	OE*	**1.39**	0.12	**0.90**	0.22	**1.52**	0.22	**1.25**	0.38	**1.51**	0.24	**0.84**	0.27
Y57:	OH	**0.37**	0.11	**1.01**	0.14	**0.37**	0.10	**1.61**	0.59	**0.42**	0.08	**1.27**	0.17
R82:	NZ	**0.88**	0.09	**0.75**	0.11	**0.96**	0.12	**0.90**	0.63	**0.88**	0.11	**0.64**	0.12
D85:	OD*	**0.31**	0.04	**1.32**	0.11	**0.30**	0.02	**1.76**	0.63	**0.29**	0.01	**1.47**	0.16
Y157:	OH	**0.43**	0.10	**1.21**	0.16	**0.45**	0.04	**1.52**	0.74	**0.51**	0.16	**1.31**	0.16
E194:	OE*	**1.07**	0.13	**0.31**	0.06	**1.41**	0.22	**0.94**	0.79	**1.19**	0.19	**0.38**	0.13
E204:	OE*	**1.12**	0.09	**0.30**	0.04	**1.16**	0.09	**0.58**	0.72	**1.25**	0.18	**0.29**	0.01
D212:	OD*	**0.29**	0.02	**1.14**	0.10	**0.29**	0.01	**1.76**	0.61	**0.30**	0.02	**1.43**	0.16
K216:	NZ	**0.47**	0.02	**1.42**	0.08	**0.46**	0.01	**1.97**	0.64	**0.48**	0.03	**1.71**	0.16
K216:	HZ	**0.38**	0.03	**1.36**	0.09	**0.37**	0.02	**1.89**	0.63	**0.40**	0.03	**1.62**	0.16

All units are in nm. Distances are given in boldface and standard deviations are given in normal font.

Table III
Average Valence Sum Contributions of Selected Ligands and the Total Valence Sums of Calcium

		Calcium ion (system:position)											
		1:P1		2:P2		3:P1		3:P2		4:P1		4:P2	
Y57:	OH	**0.11**	0.12			**0.10**	0.12			**0.04**	0.07		
D85:	OD*	**0.31**	0.14			**0.33**	0.12			**0.39**	0.07		
Y185:	OH	**0.04**	0.08			**0.01**	0.01			**0.04**	0.08		
E194:	OE*			**0.32**	0.07			**0.00**	0.03			**0.25**	0.19
E204:	OE*			**0.34**	0.06			**0.26**	0.19			**0.38**	0.07
D212:	OD*	**0.33**	0.11			**0.34**	0.09			**0.35**	0.10		
HOH*:	O	**0.93**	0.14	**0.97**	0.27	**0.98**	0.18	**1.78**		**0.93**	0.21	**0.83**	0.32
Total		**1.89**	0.10	**1.90**	0.11	**1.89**	0.10	**2.04**	0.17	**1.82**	0.13	**1.95**	0.12

The totals include small contributions from residues in addition to those listed.

suitable binding site will, among others, allow neutralization of the charge of a cation present, thus yielding a bond–valence sum close to the charge of the cation. The bond valence contributions and sums were calculated according to the method of Brown and Shannon[79] and parameters for calcium–oxygen bonds given by Brown and Wu.[80] The relation between the bond valence and the calcium–oxygen distance is given by

$$s = \left(\frac{r}{r_1}\right)^{-N} \quad (1)$$

where r_1 is the distance between the two atoms corresponding to unit valence. The parameters used for r_1 and N are 0.1909 nm and 5.4, respectively.[80] Note that in this case, the calculated bond valence sums primarily reflect the empirically derived nonbonded interaction terms within the force field and should be treated only as a relative measure. In reality, the interaction between the calcium ions and the ligating oxygen atoms will have partial bonding character, which in principle must be described quantum mechanically.

RESULTS

System stability

The placement of different numbers of calcium ions within each bR molecule had little effect on the structure of the bR molecules within the PM. In all cases, the system appeared to be stable on the time scale simulated. The total potential energy stabilized close to its final value within 1 ns. The change in the potential energy was associated with a decrease in the volume of the unit cell from an initial value of ~730 nm^3 to a value of ~688 nm^3 (−5.8%). The average backbone RMSD with respect to the starting structure was lowest in system **2** (0.15 nm). In the other simulations, all of which contained a calcium ion in the Schiff base region, the average RMSD of the backbone was slightly higher ranging from 0.17 nm for system **1** with just a single calcium ion in the region of the Schiff base to 0.2 nm for the simulations with calcium ions placed at P1, P2, and P3. The RMSD plots for the different systems are provided as supplementary material.

Binding of divalent ions: placement of calcium at putative binding sites

The results of the simulations in which calcium ions were placed at the putative binding sites, P1, P2, and P3, are summarized in Tables II and III and Figures 2–5. Table II presents the distances between the calcium ions and a number of selected atoms of key residues, flanking the putative binding sites. Table III presents the results from the analysis of bond valence. Figures 2–5 show the distribution of calcium ions inside bR for the simulations of systems **1**–**4**, respectively, together with a representative structure from the simulation of each system overlaid on the geometry of key residues (notably Tyr57, Arg82, Asp85, Glu194, Glu204, Asp212, and Lys216) in different crystal structures. In addition, in Figures 2 and 3 the distributions of oxygen atoms around the calcium ions for the duration of the simulations of systems **1** and **2** are shown.

Calcium positioned in the Schiff base region (P1)

Considering the simulations of systems **1**, **3**, and **4** together, there are 27 separate cases in which a calcium ion was positioned within a bR molecule at the site P1, that is, near the Schiff base between Asp85 and Asp212. Figure 2(A), shows the range of positions occupied by the calcium ion with respect to the protein for all copies of bR in the 20 ns simulation of system **1**. The ion placed initially in between Asp85 and Asp212 rapidly migrated to a position just above Asp 85 and Asp212 [residues **a** and **b** in Fig. 2(A)]. After the initial relaxation the position of the ion remains stable. As can be seen in Figure 2(A), the ion shows a very narrow distribution of positions in all 9 copies. The results obtained in the simulations of systems **3** (Fig. 4) and **4** (Fig. 5) are very similar.

In Figure 2(B), the positions of the oxygen atoms to which the ion is coordinated, occupied during the simulation, are shown for system **1**. The coordination of the

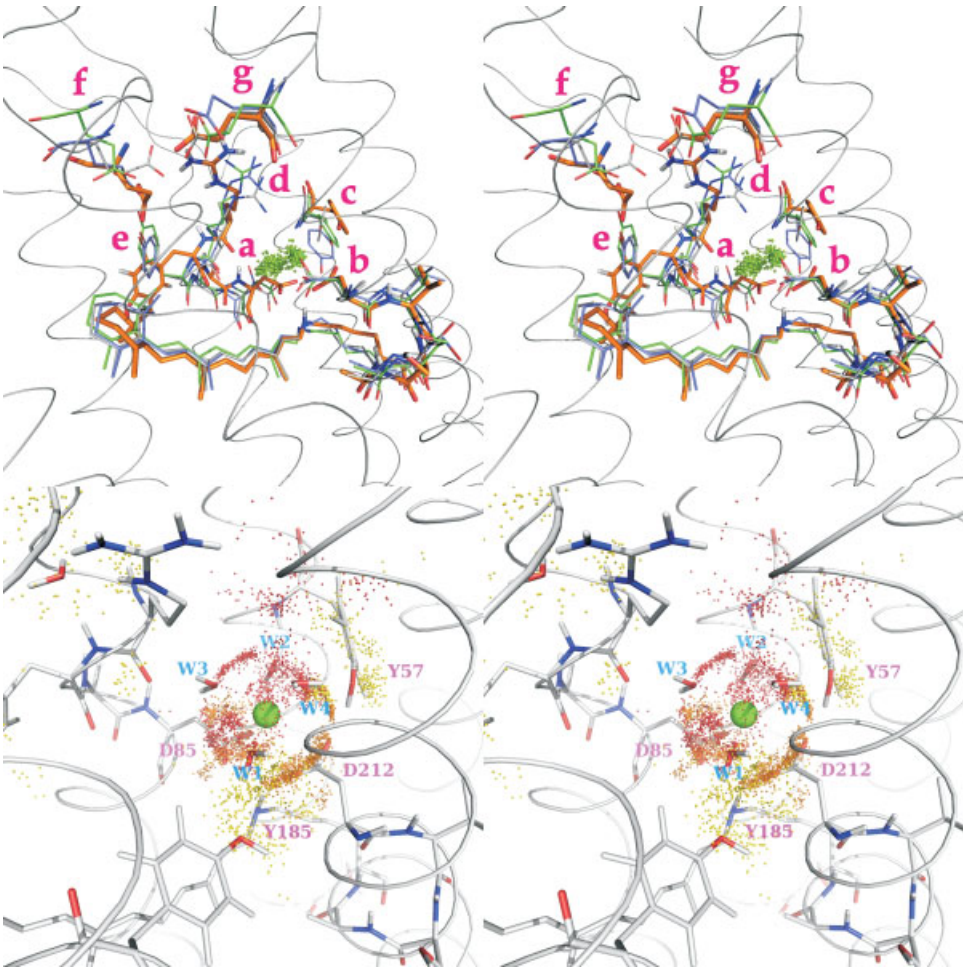

Figure 2

A cross-eyed stereoscopic image of the structural changes associated with the placement of a calcium ion at the site P1 in the region of Schiff base of bR (system **1**). (**A**) The range of positions of the calcium ions (light green) sampled during the simulation projected onto a representative structure for system **1** (shown in orange). Alternative crystal structures 1QHJ (42) (gray), 1AP9[64,65] (green), and 2AT9[25] (blue) are shown for comparison. The letters identify to the highlighted residues a. Asp85, b. Asp212, c. Tyr57, d. Arg82, e. Tyr83, f. Glu194, and g. Glu204. (**B**) The coordination of the calcium ion at P1. Amino acid ligands are labeled in magenta, water molecules in blue (arbitrary numbering).

calcium ion was primarily eightfold involving two aspartic acids, Asp85 and Asp212, the hydroxyl group of Tyr57, and three water molecules. The average valence sum of the calcium ion at P1 in system **1** was 1.89 ± 0.11 (Table III). The average valence sum contribution of the amino acid side chains was 0.93. Again, similar results were obtained for the calcium ion placed at P1 in the simulations of systems **3** and **4**.

For each system, a comparison was made between the local geometry of the Schiff base region and the proton release group and the geometry as observed in the crystal structures. To illustrate the differences and similarities between simulations and crystal structures, a single structure was extracted from the trajectories based on an analysis of the distances between selected atoms for a set of key residues listed in Table II. This structure is shown in orange in Figures 2–5. Note that, although a single structure cannot fully represent the ensemble of structures sampled during the simulation, qualitatively the same results were obtained when the distance distributions obtained from the trajectories where analyzed directly (see supplementary material). Comparing the representative structure for system **1** to the various crystal structures, several differences are evident. Asp85 (residue **a**) and Asp212 (residue **b**) are oriented more toward the calcium ion. A crystallographic water molecule, lying between Asp85 and the Schiff base is lost. There is a movement of Tyr57 (residue **c**) away from the calcium ion. The side chain of Arg82 (residue **d**) also moves to a slightly more exposed location with the guanidinium group interacting directly with the proton release group. Although significant, the deviations are not large. In

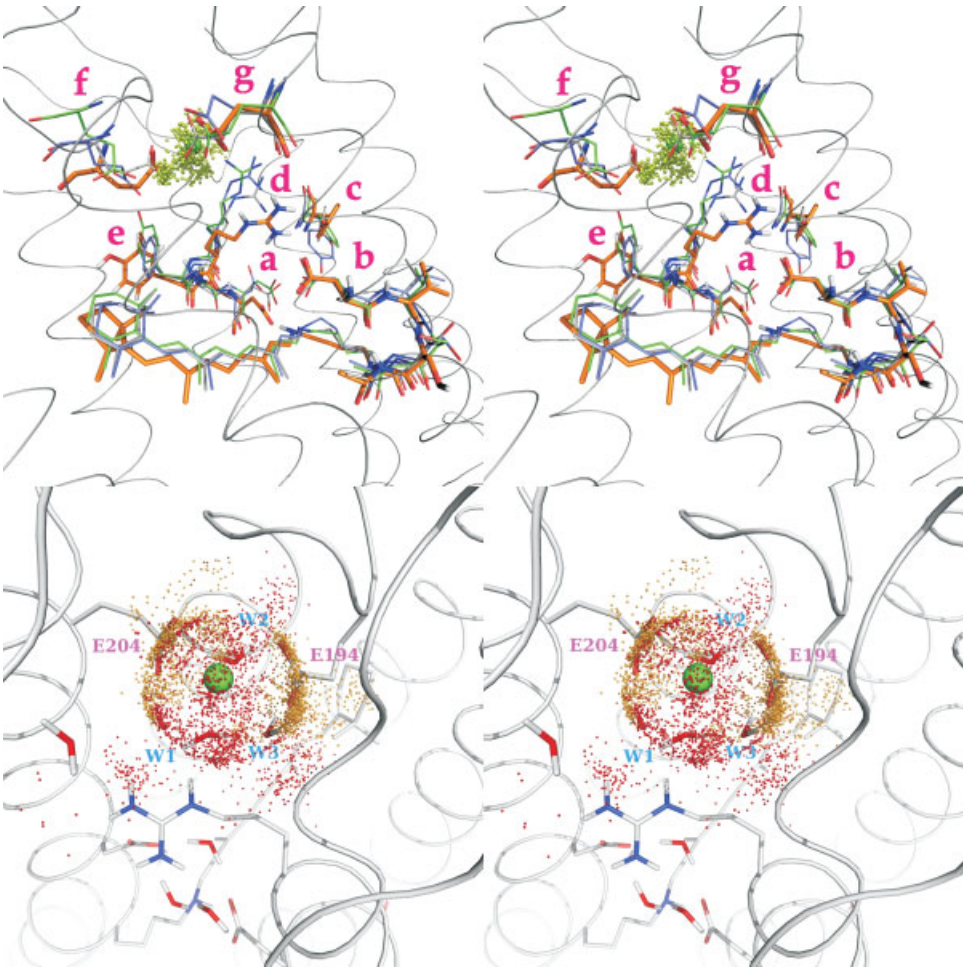

Figure 3

Structural changes associated with the placement of a calcium ion at the site P2 near the proton release group of bR with Glu194 deprotonated (system **2**). (**A**) The range of positions of the calcium ions sampled during the simulation projected onto a representative structure for system **2** together with alternate crystal structures. Labels and colors are as in Figure 2(A). (**B**) The coordination of the calcium ion at P2 in the simulation of system **2**. Labels and colors are as in Figure 2.

addition, we note that changes in the positions of Tyr83 (residue **e**) and Glu194 (residue **f**) with respect to the crystal are also evident, both becoming oriented more toward the retinal binding pocket in the simulation, even though they lie further from the position of the calcium.

In systems **3** and **4**, in addition to the calcium ion at P1, a second ion is placed near the proton release group (P2). In this case, Tyr57 (residue **c**) maintains a position close to that observed in the crystal structures (see Figs. 4 and 5). However, the guanidinium group of Arg82 (residue **d**) orients toward E9, rather than toward the proton release group. In addition, Tyr83 (residue **e**) reorients, such that the hydroxyl group interacts directly with Glu194.

Calcium positioned in between Glu194/Glu204 (P2)

Considering the simulations of systems **2**, **3**, and **4** together, there are 27 separate cases in which a calcium ion was placed near the proton release group at the site P2 between Glu194/Glu204 in bR. In systems **2** and **4** Glu194 was deprotonated, whereas in system **3** Glu194 was protonated. In addition to the calcium at P2 in the systems **3** and **4**, a calcium ion was also placed at P1 and at P3.

Figure 3 summarizes the results of the simulation of system **2**, in which a single calcium ion was positioned between the proton release groups of each bR molecule. From Figure 3(A), which shows the distribution of the calcium ion with respect to the protein, it can be seen that the ion remains in a well-defined region. This is supported by the results in Table II, which shows the average and standard deviation of the distance between the calcium and each of a set of selected atoms. In all cases the standard deviation was 0.22 nm or less. The representative configuration, for system **2** [shown in orange in Fig. 3(A)], closely matches that observed in most crystal structures of ground state bR. The most notable differen-

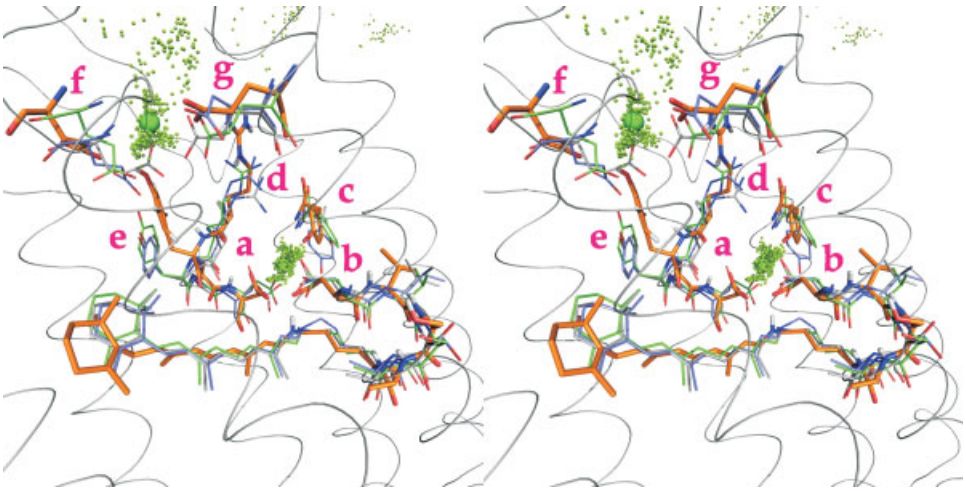

Figure 4

Structural changes associated with the placement of a calcium ion at the sites P1, P2 (Glu194 protonated), and P3 (near Glu9) in bR (system **3**). The range of positions of the calcium ions sampled during the simulation projected onto a representative structure for system **3** together with alternate crystal structures. Labels and colors are as in Figure 2.

ces are the reorientation of Asp85 (residue **a**) toward the Schiff base and a shift in the position of Arg82 (residue **d**). As observed for system **1**, the water molecule positioned between Asp85 and the Schiff base in the crystal structures was lost. From Figure 3(B), it can be seen that the calcium ion is coordinated by the residues Glu194 and Glu204, which contribute 0.32 and 0.34 to the total valence sum, respectively (Table III). In addition, the calcium is coordinated by three water molecules, which together have a valence sum contribution of 0.97 (±0.27). On an average, the total valence sum for the calcium ion in system 2 was 1.90 (±0.11).

In the case of system **3**, in which Glu194 was protonated, two out of the nine calcium ions placed at P2 escaped into the bulk solvent (Fig. 4). A further two moved to a position closer to Glu9. In only four of the nine cases did the ion remain close to the position, at which it was placed initially. Furthermore, in those cases where the ion did remain close to its initial position the local geometry of the protein became distorted. The fact

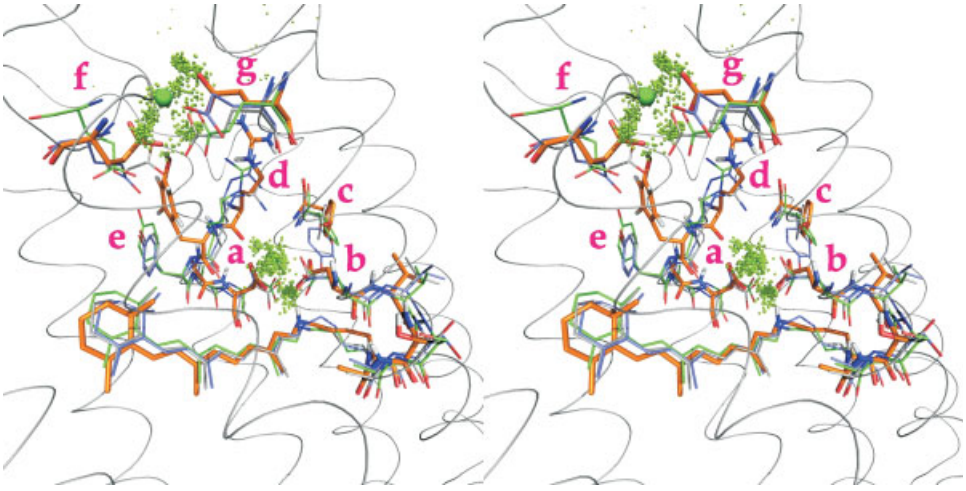

Figure 5

Structural changes associated with the placement of a calcium ion at the sites P1, P2 (Glu194 deprotonated), and P3 in bR (system **4**). The range of positions of the calcium ions sampled during the simulation projected onto a representative structure for system **4** together with alternate crystal structures. Labels and colors are as in Figure 2.

that the calcium ion placed at P2 in system **3** was not stable is reflected in the low average valence sum contribution of the glutamic acid residues (0.00 for Glu194 and 0.26 for Glu204) shown in Table III. The placing of an ion at P2 had little effect on the properties of the ion placed at P1.

In system **4**, Glu194 was deprotonated as in system **2** but otherwise identical to system **3** with calcium ions placed at P1, P2, and P3. In this case, the calcium at P2 sampled a range of positions in the general vicinity of where it was placed initially (Fig. 5). However, the distribution was much more diffuse than in system **2**. In particular, the ion interacts tightly with Glu194, which is reflected in the lower average valence sum contribution of this residue (Table III). Comparing the representative structure for system **4** to the available crystal structures, (Fig. 5) it can be seen that both Glu194 (residue **f**) and Glu204 (residue **g**) are displaced.

Calcium positioned near Glu9 (P3)

Considering simulations **3** and **4** together, there are 18 separate cases in which a calcium ion was placed near Glu9 in bR, simultaneously with one calcium near the Schiff base and a second calcium near the proton release group. In all cases, the calcium ion moved away from the proposed position (P3) during energy minimization and escaped into the solvent during the initial stages of unrestrained MD.

DISCUSSION

First, the simulations demonstrate that a calcium ion is not required to maintain the conformation of the Schiff base region (P1). The configuration of the Schiff base in the simulation of system **2**, which does not contain a calcium ion in this region, is in good agreement with that found in the majority of the high-resolution crystal structures. When a calcium ion was placed at P1 in the vicinity of the Schiff base, significant changes in the local geometry structure with respect to the available crystallographic structures were observed. In particular, Asp85 and Asp212 orient toward the calcium ion, and the hydroxyl group of Tyr57 becomes directed toward the ion. In addition, the side chain of Arg82 moves to a more external location, with the guanidinium group interacting with the proton release group. Interestingly, the configuration obtained in the simulation of system **1**, in which just a single calcium ion was placed in the Schiff base region (P1), shows similarities to the structure 1AP9[64,65] (after correction for 18% twinning). Previously, it had been argued that this structure requires the inclusion of a cation in the region of the Schiff base to account for one and two-photon spectroscopic data.[22] The present results support this hypothesis. However, although it appears possible that a calcium ion could be accommodated in the region of the Schiff base, this would be associated with changes in the local geometry not seen in the majority of crystal structures.

The simulations of systems **2** and **4** suggest that the proton release group could function as a calcium binding site. In particular, the close similarity between the results obtained from the simulation of system **2** and the majority of the available crystal structures supports this conjecture. The most significant change observed in the simulation of system **2** when compared with the crystal structures is that Arg82 is found to adopt a more inward position, interacting directly with Asp85. In most of the crystal structures, the guanidinium group of Arg82 is oriented toward Asp212. A similar effect was observed previously by Kandt *et al.*[29] who performed a simulation of bR in which the proton release group was protonated with no cations present. Another difference between system **2** and the crystal structures relates to the loss of a water molecule that hydrogen bonds to both the Schiff base and Asp85. The loss of this water molecule has also been observed in previous classical simulations.[81,82] The water appears stable if a quantum mechanical treatment is used.[29,82] Interestingly, the configuration of the Schiff base region observed in the simulation of system **2**, in which Arg82 lies closer to Asp85 then proposed in the majority of the crystal structures is in very good agreement with the model proposed by Kusnetzow *et al.*[22] to explain the results obtained from one-photon and two-photon spectroscopy.[16] By inducing a shift in the position of Arg82, the presence of a calcium ion between Glu194 and Glu204 would also affect (lower) the pK_a of Asp85. This might explain the observed coupling between cation binding and the bR absorption spectrum. It would also help to explain the other experimental results including the observation that Asp212 is more strongly coupled to calcium binding than Asp85.[6,20] It has been proposed previously that Glu194 and Glu204 coordinate a Zundel ($H_5O_2^+$) complex, which is the source of the proton being released to the bulk.[49,83] Recent evidence even suggests a more complex situation, with direct involvement of more water molecules in a protonated water cluster.[84,85] Although Zundel or Eigen complexes might only be formed transiently,[85] the simultaneous presence of a protonated water cluster and a calcium ion in the extracellular region might at first seem unlikely. In this regard, we note that that the overall charge in this region is negative due to the presence of Glu9, Glu194, and Glu204, and that the presence of both cationic species, would in fact render the interior of bR neutral.

The simulations do not support the proposal that calcium ions bind at the site P3 within the interior of bR near Glu9[26] simultaneously to calcium ions at sites P1 and P2, as calcium ions placed in this region were not stable. It is of course possible that the inclusion of polarization terms in the force field might enhance the stability of a calcium ion at this site. However, considering the very rapid loss of calcium ions from this site, it is very unlikely that even when including polarization effects a calcium ion would bind at this position. Nevertheless,

experimental results do suggest that Glu9 is involved in cation binding.[26] In this case Glu9 may act indirectly, stabilizing the structure of the extracellular region. Likewise, the simulations do not support the simultaneous placement of calcium ions in the Schiff base region and the proton release group as this resulted in more widespread destabilization of the structure of bR.

CONCLUSIONS

A series of simulations of a highly detailed model of the PM containing three bR trimers with calcium ions placed at three proposed binding sites has been performed. The simulations suggest that a single calcium ion could be accommodated either in the region of the Schiff base or the region of the proton release group but not a proposed site near Glu9 in the interior of bR. Placing a calcium ion in the region of the Schiff base gives rise to a structure, which is roughly in line with the crystal structure proposed by Pebay-Peyroula *et al.*,[64,65] but which differs significantly from the majority of crystal structures of ground state bR. When a calcium ion is placed in the region of the proton release group, the structures obtained in the simulations closely resemble the consensus crystal structure and are consistent with a range of experimental observations.[14,26,27] However, the binding of a calcium ion between the glutamate residues forming the proton release group raises questions in regard to the nature of the group that releases the proton to the bulk and whether a calcium ion and a protonated water cluster might be present simultaneously.[49,83–85]

REFERENCES

1. Oesterhelt D, Stoeckenius W. Rhodopsin-like protein from purple membrane of *Halobacterium halobium*. Nat New Biol 1971;233:149–152.
2. Chang CH, Chen JG, Govindjee R, Ebrey T. Cation binding by bacteriorhodopsin. Proc Natl Acad Sci USA 1985;82:396–400.
3. Kimura Y, Ikegami A, Stoeckenius W. Salt and pH-dependent changes of the purple membrane absorption-spectrum. Photochem Photobiol 1984;40:641–646.
4. Zhang YN, Sweetman LL, Awad ES, Elsayed MA. Nature of the individual Ca^{2+} binding-sites in Ca^{2+}-regenerated bacteriorhodopsin. Biophys J 1992;61:1201–1206.
5. Mowery PC, Lozier RH, Chae Q, Tseng YW, Taylor M, Stoeckenius W. Effect of acid pH on the absorption-spectra and photoreactions of bacteriorhodopsin. Biochemistry 1979;18:4100–4107.
6. Jonas R, Ebrey TG. Binding of a single divalent-cation directly correlates with the blue-to-purple transition in bacteriorhodopsin. Proc Natl Acad Sci USA 1991;88:149–153.
7. Subramaniam S, Marti T, Khorana HG. Protonation state of Asp (Glu)-85 regulates the purple-to-blue transition in bacteriorhodopsin mutants Arg-82----Ala and Asp-85----Glu—the blue form is inactive in proton translocation. Proc Natl Acad Sci USA 1990;87:1013–1017.
8. Metz G, Siebert F, Engelhard M. Asp (85) is the only internal aspartic-acid that gets protonated in the M-intermediate and the purple-to-blue transition of bacteriorhodopsin—a solid-state C-13 Cp-Mas Nmr investigation. FEBS Lett 1992;303:237–241.
9. Szundi I, Steckenius W. Effect of lipid surface-charges on the purple-to-blue transition of bacteriorhodopsin. Proc Natl Acad Sci USA 1987;84:3681–3684.
10. Szundi I, Stoeckenius W. Purple-to-blue transition of bacteriorhodopsin in a neutral lipid environment. Biophys J 1988;54:227–232.
11. Szundi I, Stoeckenius W. Surface pH controls purple-to-blue transition of bacteriorhodopsin—a theoretical-model of purple membrane-surface. Biophys J 1989;56:369–383.
12. Varo G, Brown LS, Needleman R, Lanyi JK. Binding of calcium ions to bacteriorhodopsin. Biophys J 1999;76:3219–3226.
13. Alexiev U, Mollaaghababa R, Scherrer P, Khorana HG, Heyn MP. Rapid long-range proton diffusion along the surface of the purple membrane and delayed proton-transfer into the bulk. Proc Natl Acad Sci USA 1995;92:372–376.
14. Eliash T, Weiner L, Ottolenghi M, Sheves M. Specific binding sites for cations in bacteriorhodopsin. Biophys J 2001;81:1155–1162.
15. Luo GM, Malkova S, Yoon J, Schultz DG, Lin BH, Meron M, Benjamin I, Vanysek P, Schlossman ML. Ion distributions near a liquid-liquid interface. Science 2006;311:216–218.
16. Stuart JA, Vought BW, Zhang CF, Birge RR. The Active-site of bacteriorhodopsin—2-photon spectroscopic evidence for a positively charged chromophore binding-site mediated by calcium. Biospectroscopy 1995;1:9–28.
17. Pardo L, Sepulcre F, Cladera J, Dunach M, Labarta A, Tejada J, Padros E. Experimental and theoretical characterization of the high-affinity cation-binding site of the purple membrane. Biophys J 1998;75:777–784.
18. Sepulcre F, Proietti MG, Benfatto M, Della Longa S, Garcia J, Padros E. A quantitative XANES analysis of the calcium high-affinity binding site of the purple membrane. Biophys J 2004;87:513–520.
19. Yang DF, ElSayed MA. The Ca^{2+} binding to deionized monomerized and to retinal removed bacteriorhodopsin. Biophys J 1995;69:2056–2059.
20. Zhang YN, Elsayed MA, Bonet ML, Lanyi JK, Chang M, Ni B, Needleman R. Effects of genetic replacements of charged and H-bonding residues in the retinal pocket on Ca^{2+} binding to deionized bacteriorhodopsin. Proc Natl Acad Sci USA 1993;90:1445–1449.
21. Sepulcre F, Cordomi A, Proietti MG, Perez JJ, Garcia J, Querol E, Padros E. X-ray absorption and molecular dynamics study of cation binding sites in the purple membrane. Proteins Struct Funct Bioinformatics 2007;67:360–374.
22. Kusnetzow A, Singh DL, Martin CH, Barani IJ, Birge RR. Nature of the chromophore binding site of bacteriorhodopsin: the potential role of Arg (82) as a principal counterion. Biophys J 1999;76:2370–2389.
23. Fu X, Bressler S, Ottolenghi M, Eliash T, Friedman N, Sheves M. Titration kinetics of Asp-85 in bacteriorhodopsin: exclusion of the retinal pocket as the color-controlling cation binding site. FEBS Lett 1997;416:167–170.
24. Eliash T, Ottolenghi M, Sheves M. The titrations of Asp-85 and of the cation binding residues in bacteriorhodopsin are not coupled. FEBS Lett 1999;447:307–310.
25. Mitsuoka K, Hirai T, Murata K, Miyazawa A, Kidera A, Kimura Y, Fujiyoshi Y. The structure of bacteriorhodopsin at 3.0 angstrom resolution based on electron crystallography: implication of the charge distribution. J Mol Biol 1999;286:861–882.
26. Sanz C, Marquez M, Peralvarez A, Elouatik S, Sepulcre F, Querol E, Lazarova T, Padros E. Contribution of extracellular Glu residues to the structure and function of bacteriorhodopsin—presence of specific cation-binding sites. J Biol Chem 2001;276:40788–40794.
27. Tuzi S, Yamaguchi S, Tanio M, Konishi H, Inoue S, Naito A, Needleman R, Lanyi JK, Saito H. Location of a cation-binding site in the loop between helices F and G of bacteriorhodopsin as studied by C-13 NMR. Biophys J 1999;76:1523–1531.
28. Grudinin S, Buldt G, Gordeliy V, Baumgaertner A. Water molecules and hydrogen-bonded networks in bacteriorhodopsin—molecular

dynamics simulations of the ground state and the M-intermediate. Biophys J 2005;88:3252–3261.
29. Kandt C, Schlitter J, Gerwert K. Dynamics of water molecules in the bacteriorhodopsin trimer in explicit lipid/water environment. Biophys J 2004;86:705–717.
30. Baudry J, Tajkhorshid E, Molnar F, Phillips J, Schulten K. Molecular dynamics study of bacteriorhodopsin and the purple membrane. J Phys Chem B 2001;105:905–918.
31. Hayashi S, Tajkhorshid E, Schulten K. Molecular dynamics simulation of bacteriorhodopsin's photoisomerization using ab initio forces for the excited chromophore. Biophys J 2003;85:1440–1449.
32. Murata K, Hoshino T, Sato Y, Hata M, Tsuda M. Unidirectional proton transfer mechanism in the L -> M -> N sequence of bacteriorhodopsin. J Mol Struct-Theochem 2003;664:125–133.
33. Bondar AN, Fischer S, Smith JC, Elstner M, Suhai S. Key role of electrostatic interactions in bacteriorhodopsin proton transfer. J Am Chem Soc 2004;126:14668–14677.
34. Lee YS, Krauss M. Dynamics of proton transfer in bacteriorhodopsin. J Am Chem Soc 2004;126:2225–2230.
35. Bondar AN, Suhai S, Fischer S, Smith JC, Elstner M. Suppression of the back proton-transfer from Asp85 to the retinal Schiff base in bacteriorhodopsin: a theoretical analysis of structural elements. J Struct Biol 2007;157:454–469.
36. Nonella M, Windemuth A, Schulten K. Structure of bacteriorhodopsin and in situ isomerization of retinal—a molecular-dynamics study. Photochem Photobiol 1991;54:937–948.
37. Edman K, Royant A, Larsson G, Jacobson F, Taylor T, van der Spoel D, Landau EM, Pebay-Peyroula E, Neutze R. Deformation of helix C in the low temperature L-intermediate of bacteriorhodopsin. J Biol Chem 2004;279:2147–2158.
38. Jang H, Crozier PS, Stevens MJ, Woolf TB. How environment supports a state: molecular dynamics simulations of two states in bacteriorhodopsin suggest lipid and water compensation. Biophys J 2004;87:129–145.
39. Shih AY, Denisov IG, Phillips JC, Sligar SG, Schulten K. Molecular dynamics simulations of discoidal bilayers assembled from truncated human lipoproteins. Biophys J 2005;88:548–556.
40. Corcelli A, Lattanzio VMT, Mascolo G, Papadia P, Fanizzi F. Lipid-protein stoichiometries in a crystalline biological membrane: NMR quantitative analysis of the lipid extract of the purple membrane. J Lipid Res 2002;43:132–140.
41. Renner C, Kessler B, Oesterhelt D. Lipid composition of integral purple membrane by H-1 and P-31 NMR. J Lipid Res 2005;46: 1755–1764.
42. Kates M, Kushwaha SC, Sprott GD. Lipids of purple membrane from extreme halophiles and of methanogenic bacteria. Methods Enzymol 1982;88:98–111.
43. DeLano WL. The pymol molecular graphics system.0.99. San Carlos, CA: DeLano Scientific; 2005.
44. Povray Development Core. Persistence of Vision Raytracer. 3.6: Persistence of Vision Raytracer Pty. Ltd; 2004.
45. Essen LO, Siegert R, Lehmann WD, Oesterhelt D. Lipid patches in membrane protein oligomers: crystal structure of the bacteriorhodopsin-lipid complex. Proc Natl Acad Sci USA 1998;95:11673–11678.
46. Belrhali H, Nollert P, Royant A, Menzel C, Rosenbusch JP, Landau EM, Pebay-Peyroula E. Protein, lipid and water organization in bacteriorhodopsin crystals: a molecular view of the purple membrana at 1.9 angstrom resolution. Structure 1999;7:909–917.
47. Luecke H, Schobert B, Richter HT, Cartailler JP, Lanyi JK. Structure of bacteriorhodopsin at 1.55 angstrom resolution. J Mol Biol 1999; 291:899–911.
48. Guex N, Peitsch MC. SWISS-MODEL and the Swiss-PdbViewer: an environment for comparative protein modeling. Electrophoresis 1997;18:2714–2723.
49. Garczarek F, Brown LS, Lanyi JK, Gerwert K. Proton binding within a membrane protein by a protonated water cluster. Proc Natl Acad Sci USA 2005;102:3633–3638.
50. Weik M, Patzelt H, Zaccai G, Oesterhelt D. Localization of glycolipids in membranes by in vivo labeling and neutron diffraction. Mol Cell 1998;1:411–419.
51. Schuttelkopf AW, van Aalten DMF. PRODRG: a tool for high-throughput crystallography of protein-ligand complexes. Acta Crystallogr Sect D: Biol Crystallogr 2004;60:1355–1363.
52. Kushner DJ. Lysis and dissolution of cells and envelopes of an extremely halophilic bacterium. J Bacteriol 1964:87:1147–1156.
53. van Gunsteren WF, Billeter SR, Eising AA, Hunenberger PH, Kruger P, Mark AE, Scott WRP, Tironi IG. Biomolecular simulation: GROMOS96 manual and user guide. Zürich, Groningen: BIOMOS BV; 1996.
54. Schuler LD, Daura X, van Gunsteren WF. An improved GROMOS96 force field for aliphatic hydrocarbons in the condensed phase. J Comput Chem 2001;22:1205–1218.
55. Lins RD, Hunenberger PH. A new GROMOS force field for hexopyranose-based carbohydrates. J Comput Chem 2005;26:1400–1412.
56. Berendsen HJC, Postma JPM, van Gunsteren WF, Hermans J. Interaction models for water in relation to protein hydration. In: Pullman B, editor. Intermolecular forces. Dordrecht: Reidel; 1981. pp 331–342.
57. Berendsen HJC, van der Spoel D, van Drunen R. Gromacs—a message-passing parallel molecular-dynamics implementation. Comput Phys Commun 1995;91:43–56.
58. Lindahl E, Hess B, van der Spoel D. GROMACS 3.0: a package for molecular simulation and trajectory analysis. J Mol Model 2001;7: 306–317.
59. van der Spoel D, van Buuren AR, Apol MEF, Meulenhoff PJ, Tieleman DP, Sijbers ALTM, Hess B, Feenstra KA, Lindahl E, van Drunen R, Berendsen HJC. Gromacs user manual version 3.1. Groningen, The Netherlands; 2002.
60. Tironi IG, Sperb R, Smith PE, van Gunsteren WF. A generalized reaction field method for molecular-dynamics simulations. J Chem Phys 1995;102:5451–5459.
61. Berendsen HJC, Postma JPM, van Gunsteren WF, DiNola A, Haak JR. Molecular-dynamics with coupling to an external bath. J Chem Phys 1984;81:3684–3690.
62. Miyamoto S, Kollman PA. Settle—an analytical version of the shake and rattle algorithm for rigid water models. J Comput Chem 1992; 13:952–962.
63. Ryckaert JP, Ciccotti G, Berendsen HJC. Numerical-integration of cartesian equations of motion of a system with constraints—molecular-dynamics of n-alkanes. J Comput Phys 1977;23:327–341.
64. PebayPeyroula E, Rummel G, Rosenbusch JP, Landau EM. X-ray structure of bacteriorhodopsin at 2.5 angstroms from microcrystals grown in lipidic cubic phases. Science 1997;277:1676–1681.
65. Royant A, Grizot S, Kahn R, Belrhali H, Fieschi F, Landau EM, Pebay-Peyroula E. Detection and characterization of merohedral twinning in two protein crystals: bacteriorhodopsin and p67phox. Acta Crystallogr Sect D 2002;58:784–791.
66. Kimura Y, Vassylyev DG, Miyazawa A, Kidera A, Matsushima M, Mitsuoka K, Murata K, Hirai T, Fujiyoshi Y. Surface of bacteriorhodopsin revealed by high-resolution electron crystallography. Nature 1997;389:206–211.
67. Luecke H, Richter HT, Lanyi JK. Proton transfer pathways in bacteriorhodopsin at 2.3 Å resolution. Science 1998;280:1934–1937.
68. Subramaniam S, Henderson R. Molecular mechanism of vectorial proton translocation by bacteriorhodopsin. Nature 2000;406:653–657.
69. Matsui Y, Sakai K, Murakami M, Shiro Y, Adachi S, Okumura H, Kouyama T. Specific damage induced by X-ray radiation and structural changes in the primary photoreaction of bacteriorhodopsin. J Mol Biol 2002;324:469–481.
70. Facciotti MT, Rouhani S, Burkard FT, Betancourt FM, Downing KH, Rose RB, McDermott G, Glaeser RM. Structure of an early intermediate in the M-state phase of the bacteriorhodopsin photocycle. Biophys J 2001;81:3442–3455.

71. Schobert B, Cupp-Vickery J, Hornak V, Smith SO, Lanyi JK. Crystallographic structure of the K intermediate of bacteriorhodopsin: conservation of free energy after photoisomerization of the retinal. J Mol Biol 2002;321:715–726.
72. Faham S, Yang D, Bare E, Yohannan S, Whitelegge JP, Bowie JU. Side-chain contributions to membrane protein structure and stability. J Mol Biol 2004;335:297–305.
73. Takeda K, Sato H, Hino T, Kono M, Fukuda K, Sakurai I, Okada T, Kouyama T. A novel three-dimensional crystal of bacteriorhodopsin obtained by successive fusion of the vesicular assemblies. J Mol Biol 1998;283:463–474.
74. Faham S, Boulting GL, Massey EA, Yohannan S, Yang D, Bowie JU. Crystallization of bacteriorhodopsin from bicelle formulations at room temperature. Protein Sci 2005;14:836–840.
75. Grigorieff N, Ceska TA, Downing KH, Baldwin JM, Henderson R. Electron-crystallographic refinement of the structure of bacteriorhodopsin. J Mol Biol 1996;259:393–421.
76. Pauling L. The principles determining the structure of complex ionic crystals. J Am Chem Soc 1929:51:1010–1026.
77. Nayal M, Di Cera E. Predicting Ca^{2+} binding sites in proteins. Proc Natl Acad Sci USA 1994:91:817–821.
78. Kombo DC, Young MA, Beveridge DL. Molecular dynamics simulation accurately predicts the experimentally-observed distributions of the (C, N, O) protein atoms around water molecules and sodium ions. Protein Struct Funct Genet 2000:39:212–215.
79. Brown ID, Shannon RD. Empirical bond-strength bond-length curves for oxides. Acta Crystallogr Sect A 1973;29:266–282.
80. Brown ID, Wu KK. Empirical parameters for calculating cation-oxygen bond valences. Acta Crystallogr Sect B Struct Sci 1976;32:1957–1959.
81. Hayashi S, Ohmine I. Proton transfer in bacteriorhodopsin: structure, excitation, IR spectra, and potential energy surface analyses by an ab initio QM/MM method. J Phys Chem B 2000;104:10678–10691.
82. Hayashi S, Tajkhorshid E, Schulten K. Structural changes during the formation of early intermediates in the bacteriorhodopsin photocycle. Biophys J 2002;83:1281–1297.
83. Spassov VZ, Luecke H, Gerwert K, Bashford D. pK(a) calculations suggest storage of an excess proton in a hydrogen-bonded water network in bacteriorhodopsin. J Mol Biol 2001;312:203–219.
84. Garczarek F, Gerwert K. Functional waters in intraprotein proton transfer monitored by FTIR difference spectroscopy. Nature 2006; 439:109–112.
85. Mathias G, Marx D. Structures and spectral signatures of protonated water networks in bacteriorhodopsin. Proc Natl Acad Sci USA 2007;104:6980–6985.